remote sensing

MDPI

Article

Mapping Cover Crops and Winter Land Cover in Michigan Using Sentinel-1 and Sentinel-2 Imagery and Google Earth Engine

Yiwen Shao †, Victor Hugo Rohden Prudente †, Jennifer Blesh, Haoyu Wang, Preeti Rao and Meha Jain *

School for Environment and Sustainability, University of Michigan, Ann Arbor, MI 48109, USA; shaoyw@umich.edu (Y.S.); victorrp@umich.edu (V.H.R.P.); hywong@umich.edu (H.W.); rpreeti@umich.edu (P.R.)
* Correspondence: mehajain@umich.edu
† These authors contributed equally to this work.

Highlights

What are the main findings?

- We find that Sentinel-1 and Sentinel-2 data can be used to effectively map winter land cover, including cover crops, in the Midwestern United States.
- We are able to map cover crop species with moderate accuracy.

What are the implications of the main findings?

- These results have important implications for understanding the extent of cover crop adoption across large-scale farming systems.
- While our models performed moderately well across heterogeneous regions, more work is needed to understand the results' generalizability.

Abstract

In temperate climates, diversifying rotations with overwintering cover crops provides many benefits, including reducing nutrient losses, restoring soil organic matter, and managing weeds. However, there is limited understanding of where and when cover crops have been planted, especially relative to harvested winter crops, such as wheat and alfalfa. In this study, we use Sentinel-1 and Sentinel-2 satellite data to map winter land cover, including cover crops, across three sites in the Lower Peninsula of Michigan using random forest models. Our results show overall moderate accuracy (60–80%) across all three sites, with individual-level accuracies varying by region and land cover type. Generally, models that combined Sentinel-1 and Sentinel-2 bands, polarizations, and indices performed better than models that relied on one sensor alone. F1 scores for cover crop mapping were moderate, with the highest accuracies achieved for mapping any cover crop (0.77) compared to individual cover crop species—cereal rye (0.72) or ryegrass (0.50). Considering which bands and time periods were the most important for the classification, we found that vegetation indices developed using the red edge bands in the earlier part of the growing season were particularly important for classification accuracy. This work suggests that readily available Sentinel-1 and Sentinel-2 satellite data can be used to accurately map winter land cover, including cover crops, in the US Midwest.

Keywords: cover crops; cereal rye; ryegrass; Michigan; Sentinel-1; Sentinel-2; random forest

Check for updates

Academic Editors: Luo Liu, Jilin Yang, Fei Li, Yaqun Liu and Wenzhi Zhao

Received: 16 February 2026
Revised: 15 May 2026
Accepted: 9 June 2026
Published: 11 June 2026

Copyright: © 2026 by the authors. Licensee MDPI, Basel, Switzerland. This article is an open access article distributed under the terms and conditions of the Creative Commons Attribution (CC BY) license.

1. Introduction

Agricultural intensification has led to significant environmental externalities, including soil erosion, groundwater depletion, and eutrophication [1,2]. Such negative environmental externalities are particularly acute in the row crop systems found in the Midwestern United States. In this region, a combination of low crop diversity, excess fertilizer input, tile drainage, and winter bare fallow periods (i.e., the 4–8 months when no living plants are in agricultural fields following harvest) has led to nutrient losses that cause hypoxic conditions in the Gulf of Mexico [3,4] and harmful algal blooms in the Great Lakes [5,6]. These undesirable consequences of conventional agriculture have prompted the adoption of more sustainable agricultural practices, including diversifying crop rotations with species that can replace winter bare fallows and fill distinct functional niches, such as winter small grains, perennial forages (e.g., alfalfa), and non-harvested overwintering cover crops [7–9].

Diverse crop rotations can reduce nutrient losses, build soil organic matter, and increase resilience to a changing climate [8,10,11]. For instance, cover crops have been shown to mitigate soil erosion, reduce surface runoff, improve water infiltration, retain soil moisture, and suppress weeds [12]. Overwintering cover crops such as cereal rye can be planted in the off-season between primary crops in rotation. Overall, cover crops are gaining renewed attention with adoption in the U.S. Midwest increasing from 1.8% to 7.2% between 2011 and 2021 [13], in part due to increases in financial incentives [14–16]. Winter crops that are harvested, such as wheat and alfalfa, are well-characterized in existing datasets, such as the Cropland Data Layer (CDL) provided by the United States Department of Agriculture (USDA); however, to date it has been challenging to track where and when cover crops have been adopted, especially for particular cover crop species. It is also challenging to determine whether farmers continue to use cover crops through time because typical methods such as censuses do not capture spatially explicit annual data.

Remote sensing offers a viable way to map cover crop characteristics at large spatial and temporal scales at low cost [17]. Previous studies have used satellite data to map cover crops in multiple regions across the globe, including the United States, Europe, South America, and East Asia [18–21]. These studies have focused on mapping the presence or absence of any cover crop [13,22,23], cover crop phenology [24], and cover crop biomass [25]. Most studies have relied on using multi-spectral optical imagery, though some recent studies have also included thermal imagery [25,26]. Previous studies have largely mapped cover crop presence or absence by detecting vegetation biomass using vegetation indices from moderate resolution imagery, such as Landsat and Sentinel-2, outside of the agricultural growing season (e.g., Hively et al., [17]; Seifert et al., [20]) or by assessing crop cover phenology [27]. Other studies have used vegetation indices from high temporal resolution imagery, such as MODIS, to map the phenology of cover crops, including their sowing and termination dates [28,29]. Finally, other studies have used peak vegetation indices throughout the growing season to estimate cover crop biomass and performance [30–32].

While previous studies have largely mapped the presence or absence of any cover crop, it remains unclear (1) how effectively key cover crop species (e.g., cereal rye) can be mapped. Mapping not just general winter cover but specific species is important because different winter cover species can have different impacts on soil health, nutrient retention, and crop yields [33,34]. Recent work has shown that locally calibrated random forest models using Sentinel-2 satellite data can distinguish functional cover crop types, with overall accuracies around 83%, though species-level classification remains challenging due to variable biomass and phenological overlap [21]. Red edge bands (B5, B6, B7) and tillage indices have proven particularly valuable for separating different winter cover types [21]. More broadly, optical bands are sensitive to different aspects of crop physiology: visible and red edge bands respond to chlorophyll absorption, while SWIR bands capture water

content and biochemical components such as cellulose and lignin [35]. More work is needed to better identify how well individual winter cover types, particularly individual cover crop species, can be mapped at scale.

Furthermore, most studies in North America have relied on using only optical imagery to map cover crop presence [13,17,20,21,36], and it remains unclear whether (2) including radar data can improve model prediction accuracy. It is possible that a combination of radar and optical data could offer more promise by providing data during typically cloudy periods in the spring that are important for detecting cover crop growth. This is because optical satellite data cannot provide high-quality imagery during periods of high cloud cover, while radar data can penetrate clouds and provide information about vegetation growth during these periods, through measures such as the radar vegetation index (RVIm). Radar is sensitive to the geometry and water content of vegetation making it especially valuable for mapping winter crops in regions with frequent spring cloud cover such as Michigan [23]. Furthermore, radar satellite data also provide a measure of surface roughness that may help distinguish different winter cover types based on different backscatter intensities (e.g., VV and VH polarizations). Previous studies have shown that crop type can be more accurately mapped when using a combination of radar and optical imagery [37–39]. Furthermore, work in Europe has shown that radar data alone can be used to map cover crop presence during periods of high cloud cover [23,40] and models that combine radar and optical imagery result in even higher accuracy [41].

In this study, we used Sentinel-1 radar and Sentinel-2 optical satellite data to classify winter cover types, including cover crop species, in the Lower Peninsula of Michigan. We specifically ask the following research questions:

(1) How effectively can Sentinel-1 and/or Sentinel-2 map winter cover types, including cover crop species, across multiple regions in Michigan? Does the inclusion of radar data along with optical imagery improve winter cover prediction accuracy?
(2) Can we develop a state-level algorithm that maps winter cover types accurately across multiple sites with varying climate, farm management practices, and soil types?
(3) Which bands, polarizations, indices, and time periods are most important for classifying winter cover types? Do radar vegetation indices and/or backscatter intensity improve on models that rely solely on optical bands and indices?

Our study provides important insights into the ability of readily available Sentinel-1 and Sentinel-2 satellite imagery to distinguish and map distinct winter cover types, including cover crops, across Michigan and the Midwestern United States more broadly.

2. Methods

2.1. Study Area

The study area was divided into three regions in the Lower Peninsula of Michigan (Figure 1): the southwest region (SW) spreads over three counties (Van Buren, St. Joseph, and a portion of Berrien), the southeast region (SE) contains two counties (Lenawee and Monroe), and the thumb region (TB) comprises five counties (portions of Huron, Tuscola, Sanilac, Lapeer, and St. Clair). We selected these three regions because they contain counties with relatively large land areas planted under cover crops according to the 2017 USDA census of agriculture (e.g., from 5 to 27% of agricultural land) and span contrasting climate conditions, soil types, and management systems. Prior to initiating data collection, we met with extension agents from Michigan State University and district conservationists in each region to ensure that cover crops were planted in these selected regions. The two clusters in southern Michigan (SW and SE) have high-input row crop production systems that are significant sources of nitrogen and phosphorus losses that cause eutrophication of the Great Lakes. The SW region has sandier soil types, while the SE region has heavier, clay

soils. The TB region of Michigan has a growing presence of large-scale grain farms but also has dairy production and the largest cluster of organic grain farmers in the state.

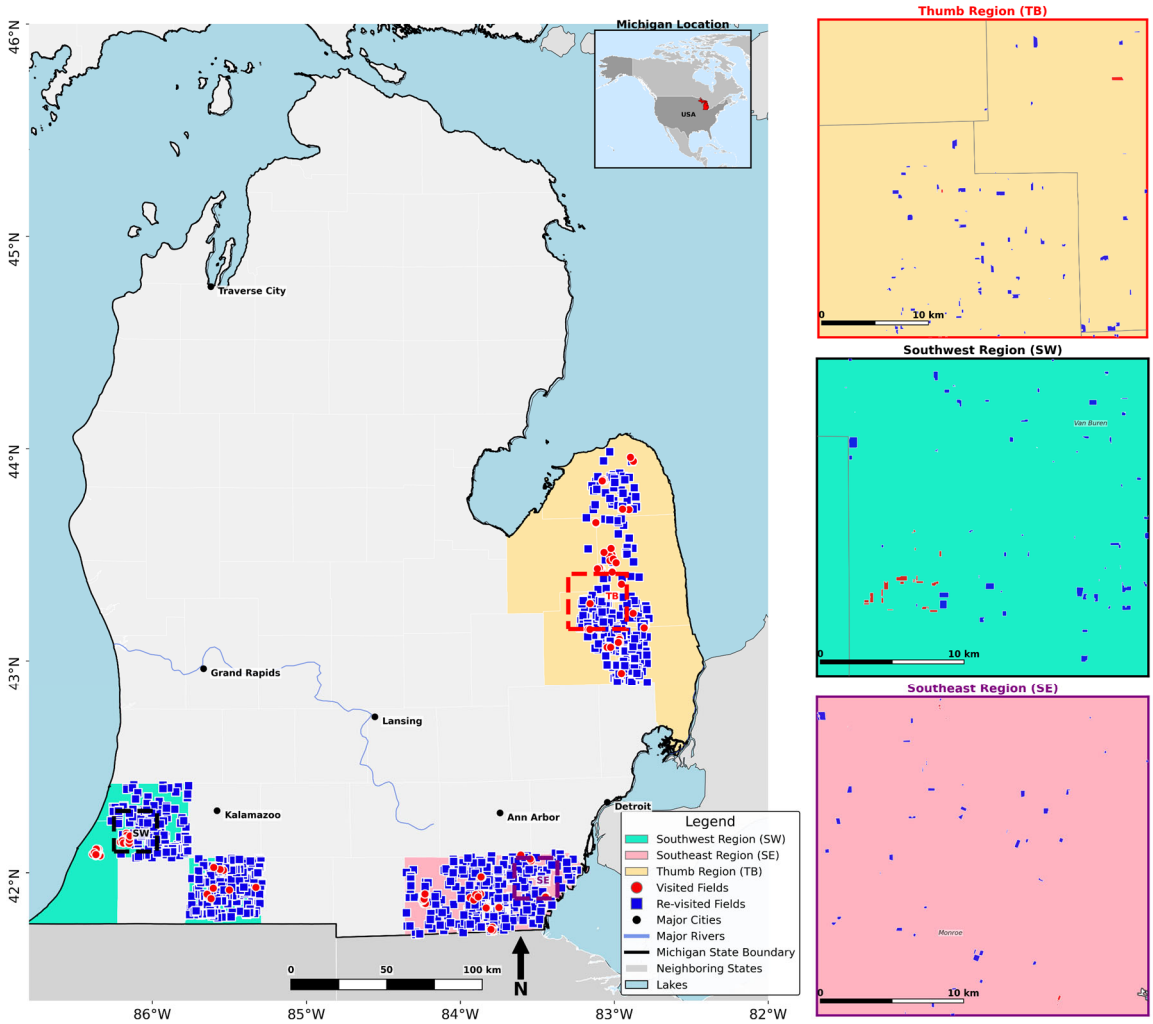


Figure 1. The three study regions: southwest (SW), southeast (SE), and the thumb (TB). The red symbols denote the fields visited in April–June 2019 and the blue symbols are the fields revisited in July to distinguish between winter wheat and cereal rye cover crop fields.

2.2. Field Data

We conducted field surveys in three stages across the three regions during April to July 2019. The field data was originally detailed by Shao [42]. During the first stage of data collection (24 April–3 May), we visited known cover crop locations using information provided by extension agents, researchers, and farmers. Extension contacts in each region shared information about our project through e-lists and newsletters, and farmers submitted field addresses or GPS points of fields with annual cover crops. For all three stages, data were collected using either handheld GPS units (Garmin eTrex 20), or the ArcCollector app (https://www.esri.com/en-us/arcgis/products/collector-for-arcgis/overview, accessed on 20 April 2019). Each field was classified by visual interpretation of the existing land cover type, with crops identified and assigned confidence levels to indicate certainty of identification (scale of 1 to 5, with 5 being highly certain). During the second stage of data collection (3 May–2 June), we revisited all three regions to collect GPS points systematically for all types of winter vegetation cover. Specifically, field teams visited 320 pre-selected points per region, which were spatially distributed throughout each region. These points were selected using a stratified random sampling approach. First, we obtained

Sentinel-2 imagery for the start of the cover crop growing season (from 1 to 28 April 2019) prior to our field survey and calculated maximum normalized difference vegetation index (NDVI) [43] for each pixel. Next, we used the 2018 cultivated layer from the USDA, National Agricultural Statistics Service (NASS) Cropland Data Layer (CDL) [44] to mask out non-agricultural areas. We then examined histograms of NDVI for the unmasked pixels across our three study regions, and binned NDVI values into four relatively equal categories (<0.2, 0.2–0.4, 0.4–0.6 and >0.6). We next used a road layer and selected 80 points per NDVI class that were within 50 m of a road, resulting in 320 points per study region. Point sampling was conducted using ArcGIS software (version 10.7). In the third stage of data collection during the first week of July (1–7 July), we revisited and confirmed field classifications for cereal rye (typically grown as a cover crop) and winter wheat (typically a harvested crop), given that these two vegetation classes had similar appearance during the first two stages of data collection (Figure 1).

To digitize field boundaries, we overlaid the collected GPS points on high-resolution Google Earth imagery and manually digitized field boundaries using visual interpretation of field edges. We excluded field polygons where the confidence level of crop identification was 3 and below. The total number of fields that remained were 345 in SE, 438 in SW, and 371 in TB, resulting in 1154 fields in total. We removed land cover classes that had few fields, reducing our total sample size to 1054 polygons (SW: 401, TB: 334, and SE: 319). This final dataset included seven different land cover types: three main types of harvested crops (alfalfa, hay forage/pasture, and winter wheat), two non-harvested cover crops (cereal rye, ryegrass), and two other common winter covers (bare/tilled, weeds, Figure 2). We were particularly interested in the accuracies when mapping the two cover crop species present in our dataset, cereal rye and ryegrass.

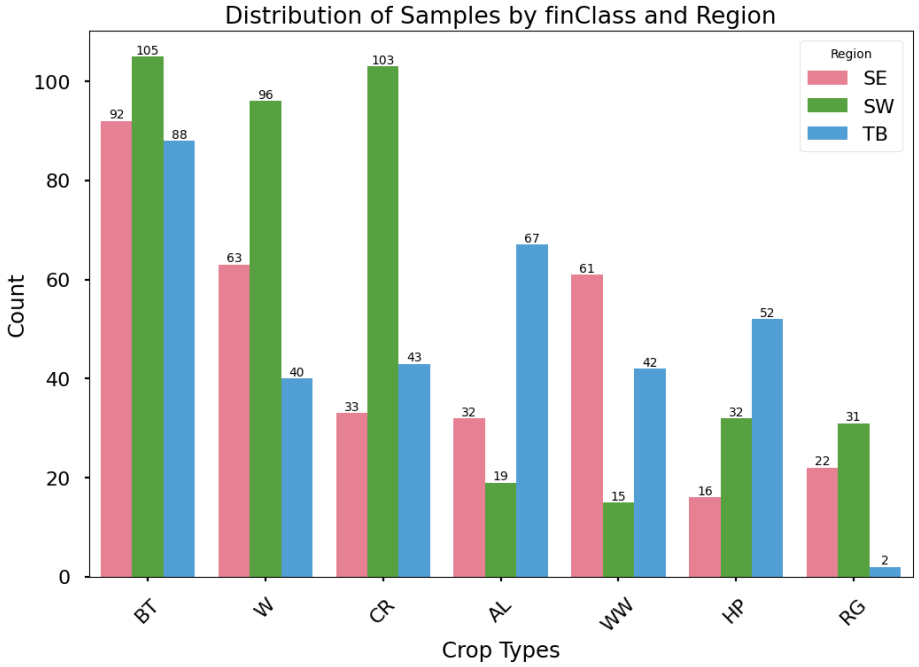


Figure 2. Bar plots showing the counts of different winter land cover types in sampled fields for the three regions. BT= bare/tilled, W = weeds, CR = cereal rye, AL = alfalfa, WW = winter wheat, HP = hay forage/pasture, and RG = ryegrass.

2.3. Satellite Data and Preprocessing

We accessed and processed Sentinel-2 surface reflectance and Sentinel-1 Ground Range Detected (GRD) satellite data using Google Earth Engine (GEE) [45]. For both satellites, we used the interval from 15 March to 31 July to cover the main cover crop growing season.

For Sentinel-2 we excluded Bands 1 (Aerosols) and 9 (Water Vapor) from our analysis as these bands represent atmospheric instead of land cover conditions. To avoid excluding usable data, the cloud filter parameter at the tile scale was set to 100% so that all available images were used. We then used the s2cloudless method [46,47] to remove cloud and cloud shadow pixels. The approach used Sentinel-2 cloud probability scores, and we excluded any pixel with a value greater than 20%. We chose 20% as a threshold value after thorough visual inspection of cloud removal accuracy using different threshold values. We then selected the pixel with the maximum NDVI value within each temporal window using the qualityMosaic function in GEE (https://developers.google.com/earth-engine/apidocs/ee-imagecollection-qualitymosaic, accessed on 20 April 2019). We created biweekly and monthly temporal mosaics, which had relatively high data availability across the three regions (Figures S1 and S2). We selected nine spectral bands from the Sentinel-2 dataset and calculated twelve spectral indices (Table 1) that have been shown to be important for monitoring agricultural crop characteristics in the previous literature.

For Sentinel-1 SAR, we preprocessed the imagery using methods from Mullissa et al. [48] (2021; https://github.com/adugnag/gee_s1_ard, accessed on 20 April 2019). We applied the Refined Lee filter (3×3) to reduce speckle effects. We calculated and extracted the linear VV and VH polarization, the cross ratio, and RVIm (Radar Vegetation Index modified, Table 1). We created 12-day quality mosaics so that image dates were consistent across regions using the qualityMosaic function in GEE based on maximum VV polarization. One image date was missing for the SE region in the beginning of June due to a gap in the Sentinel-1 tiles for this region (Figure S3).

For all bands, indices, and polarizations, we extracted the mean value for each polygon, for each period, and for each sensor. We only extracted data if at least 50% of the pixels were clear and cloud-free. All band math and data extraction at the field scale was performed using the Python (version 3.13.5) GEE (version 1.6.2) interface.

Table 1. Polarizations, spectral bands and vegetation indices used for classification. The first two columns in gray represent the bands (Sentinel-2) and polarizations (Sentinel-1) used directly from the satellite data products. The four columns on the right represent the derived indices that were calculated along with the respective formulas, description of what is measured, and references.

Band/Pol	Description	Index	Calculation	Description	References
		Sentinel-2			
B2	Blue (B)	Normalized difference vegetation index (NDVI)	(NIR − R)/(NIR + R)	Leaf area index	[49]
B3	Green (G)	Green-blue NDVI (GBNDVI)	(NIR − (G + B))/(NIR + (G + B))	Leaf area index	[50]
B4	Red (R)	Green-red NDVI (GRNDVI)	(NIR − (G + R))/(NIR + (G + R))	Leaf area index	[51]
B5	Red edge 1 (RE1)	Red edge normalized difference index (NDI)	(RE1 − R)/(RE1 + R)	Leaf area index	[52]
B6	Red edge 2 (RE2)	Plant senescence reflectance index (PSRI)	(R − G)/RE2	Plant senescence	[53]
B7	Red edge 3 (RE3)	NIR-green NDVI (NGNDVI)	(NIR − G)/(NIR + G)	Plant senescence	[54]
B8	Near-infrared (NIR)	Red edge chlorophyll index (CIre)	RE3/RE1 − 1	Leaf chlorophyll	[55]
B8A	Red edge 4 (RE4)	Green chlorophyll vegetation index (GCVI)	NIR/G − 1	Leaf chlorophyll	[55]
B11	Shortwave infrared 1 (SWIR1)	Normalized pigment chlorophyll ratio index (NPCI)	(R − B)/(R + B)	Leaf chlorophyll	[56]
B12	Shortwave infrared 2 (SWIR2)	Shortwave infrared water stress index 1 (SIWSI1)	(NIR − SWIR1)/(NIR + SWIR1)	Vegetation moisture	[57]
		Shortwave infrared water stress index 2 (SIWSI2)	(NIR − SWIR2)/(NIR + SWIR2)	Vegetation moisture	[57]
		Normalized difference tillage index (NDTI)	(SWIR1 − SWIR2)/(SWIR1 + SWIR2)	Residue cover	[58]
		Sentinel-1			
VV	Vertical–vertical polarization	VVVH ratio	VV/VH	Land cover structure	[48]
VH	Vertical–horizontal polarization	Radar Vegetation Index modified (RVIm)	(4 × VH)/(VV + VH)	Land cover structure	[59]

2.4. Scenarios and Classification Model

We calculated the percent of fields with data available for each biweekly and monthly temporal mosaic for each region, and only retained those temporal mosaics that had fewer than 50 polygons with missing data (Figures S1–S3).

Considering Sentinel-2, this resulted in monthly mosaics available for all regions and time periods, and six biweekly (14 day) mosaics for the SW region and eight biweekly mosaics for the TB and SE regions (Table 2). Considering Sentinel-1, all regions had all 12-day mosaic windows available except for the SE region, which was missing one composite at the end of May (Figure S3 and Table 2). When developing state-level models, we only used the temporal mosaic windows that were common across all three regions (Table 2).

Table 2. Monthly and biweekly time periods with available data for each region. Each date represents the start of the biweekly (14-day) and monthly composite window for Sentinel-2, and the biweekly (12-day) composite window for Sentinel-1.

Sentinel-2—14 Days			
State	**SW**	**TB**	**SE**
26 March	26 March	26 March	26 March
23 April	23 April	9 April	9 April
21 May	21 May	23 April	23 April
18 June	4 June	21 May	21 May
2 July	18 June	4 June	18 June
	2 July	18 June	2 July
		2 July	16 July
		16 July	30 July
Sentinel-2—Monthly			
1 March	1 March	1 March	1 March
1 April	1 April	1 April	1 April
1 May	1 May	1 May	1 May
1 June	1 June	1 June	1 June
1 July	1 July	1 July	1 July
Sentinel-1–12 Days			
26 March	26 March	26 March	26 March
7 April	7 April	7 April	7 April
19 April	19 April	19 April	19 April
1 May	1 May	1 May	1 May
13 May	13 May	13 May	13 May
6 June	25 May	25 May	6 June
18 June	6 June	6 June	18 June
30 June	18 June	18 June	30 June
12 July	30 June	30 June	12 July
24 July	12 July	12 July	24 July
	24 July	24 July	

We then compared multiple scenarios to understand the benefit of using Sentinel-1 versus Sentinel-2 and biweekly versus monthly composites of Sentinel-2. These scenarios were built for each region and at the state level to understand whether an accurate state-level model could be developed. Specifically, we compared five sets of models: those trained using (1) Sentinel-1 data only, (2) biweekly Sentinel-2 data only, (3) both Sentinel-1 and biweekly Sentinel-2 data, (4) monthly Sentinel-2 data only, and (5) both Sentinel-1 and monthly Sentinel-2 data (Table 3).

Table 3. Five different model scenarios examined.

Models		Temporal Aggregation
1	Sentinel-1	12-day (biweekly)
2	Sentinel-2	14-day (biweekly)
3		Monthly
4	Sentinel-1 + Sentinel-2	S1 12-day + S2 14-day
5		S1 12-day + monthly S2

We used random forest (RF), an ensemble tree-based classifier that is commonly used to map land cover, to classify winter cover types in this study [60]. We created regional models for each of the three regions (TB, SE, and SW), and one state (combined) model for all regions together. Each of the model scenarios described in Table 3 were run for each of the three regions and for the state-level model, resulting in a total of 20 models that were developed and compared.

We separated our ground truth polygons into 70% used for training and 30% used for validation across all models using stratified random sampling, which preserves the original class proportions in both subsets. This ensures that minority classes are represented in both training and validation datasets at the same relative frequency as in the full dataset. The same 30% of polygons were used as validation across all models to ensure comparability. The random forest models were run using consistent parameters across all models/scenarios. We used the standard configuration to run random forest in the scikit-learn package [61] (n_estimators = 100, max_depth = None, max_features = 'sqrt', criterion = 'gini', min_samples_split = 2, min_samples_leaf = 1, bootstrap = True, random_state = 42) in Python (version 3.13.5). Given that cereal rye and ryegrass are functionally similar cover crops (i.e., winter annual grasses), we also assessed the accuracy of our models when these two cover crop species were grouped together as one winter cover class.

We used common metrics for validation, including overall accuracy (OA), producer's accuracy (PA), user's accuracy (UA), and F1 scores [62–66]. In addition, we assessed the variable importance for each of the random forest models using the Gini importance metric. We also compared the accuracy of our cover crop predictions to those produced from the USDA's Cropland Data Layer [44], the most widely used crop type data product for the USA. To do this, we extracted the majority CDL crop class for each field polygon using zonal statistics.

3. Results

3.1. SAR and Optical Accuracies to Map Winter Crops at Local and State Levels

We found that model performance varied based on region (Table 4), and that regional models that combined Sentinel-1 and Sentinel-2 data performed best, especially with monthly Sentinel-2 mosaics.

Table 4. Overall accuracies for each of the models and regions. The best performing model for each region is bolded.

	State	SW	SE	TB
Sentinel-1 biweekly	0.5591	0.5426	0.5875	0.6500
Sentinel-2 biweekly	**0.6654**	0.6170	0.5125	0.7875
Sentinel-2 monthly	0.6457	0.5957	0.5500	0.7500
Sentinel-1 biweekly + Sentinel-2 biweekly	0.6417	**0.6489**	0.5750	0.7875
Sentinel-1 biweekly + Sentinel-2 monthly	0.6299	0.6064	**0.6000**	**0.8000**

Considering our first question that examined how well Sentinel-1 and Sentinel-2 data can map winter cover types, we found that models that combined Sentinel-1 and Sentinel-2 satellite data performed best. Specifically, the highest accuracies in the SE and TB were achieved by combining Sentinel-1 biweekly (12 days) and Sentinel-2 monthly quality mosaics (Table 4). For the SW region, the combination of Sentinel-1 (12 days) and Sentinel-2 (14 days) biweekly mosaics led to the highest accuracies. Generally, models that used only Sentinel-1 biweekly quality mosaics performed the worst, with accuracy 0.1 to 0.15 lower than the best performing model. Accuracies also varied across regions: the highest accuracy was achieved in the TB region (0.80) and the lowest accuracy occurred in the SE region (0.60). Overall, we were able to classify winter cover types with moderate accuracies using both Sentinel-1 and Sentinel-2 data in multiple sites across Michigan.

With respect to our second question, we found that a state-level algorithm performed better than some regions but worse than others. We also found that when considering state-level results, the model that used only Sentinel-2 biweekly composites performed best, but its accuracy was close to the accuracy of all other models, except for the one that used only Sentinel-1 data.

Considering the accuracy of individual land cover types, Figure 3 presents the F1 scores for each land cover type in each region and for each model (see Table S1 for more precise numbers) and Figure S8 presents user and producer's accuracies. Some cover classes had high accuracies across most models, especially the harvested crops, alfalfa (A) and winter wheat (WW), as well as bare/tilled (BT) soil. Other classes with more variable biomass, including weeds (W), hay/pasture (HP), cereal rye (CR), and ryegrass (RG), had mixed results, with high accuracies in some locations and low accuracies in other locations.

Classifying non-harvested cover crops was a main goal of our analysis, therefore we focus our results and discussion on the accuracy of mapping the cover crops considered in our study—cereal rye (CR), ryegrass (RG), and overwintering cover crops (CC), which included the cereal rye and ryegrass classes grouped together. We found that cereal rye can be classified with moderate accuracies, with F1 scores reaching 0.72 in SW (PA = 0.82, UA = 0.64; Figure S8) and 0.73 in TB (PA = 0.73, UA = 0.73; Figure S9). The high producer's accuracy in the SW indicates that most cereal rye fields were correctly detected, while the lower user's accuracy suggests some commission errors.

Ryegrass, however, was more difficult to classify, with the best performing models having F1 scores only reaching 0.5 in the SE (PA = 0.33, UA = 1.00, Figure S8) and state models (PA = 0.33, UA = 1.00, Figure S8). Notably, the user's accuracy of 1.00 indicates that when ryegrass was predicted, it was always correct, but the low producer's accuracy of 0.33 reveals that the model failed to detect most actual ryegrass fields, a systematic omission rather than commission error. It is important to note that we could not classify ryegrass in the TB region as we had only two polygons for this class available in this region.

Considering the grouped together overwintering cover crop class (Figure 3), we achieved higher accuracies than for either individual cover crop species in the state (F1: 0.64) and SW (F1: 0.77) models. Accuracies remained the same for the TB region as we were unable to classify ryegrass in that region, and accuracy for mapping ryegrass (F1: 0.5) was higher than that for the combined cover class (F1: 0.40) in the SE region. Considering which satellite data products led to the highest accuracies, models that used biweekly Sentinel-2 data typically performed best (except for in the TB region) and those that also included Sentinel-1 data saw increased improvement (except for the state models, and for the SW region for cereal rye).

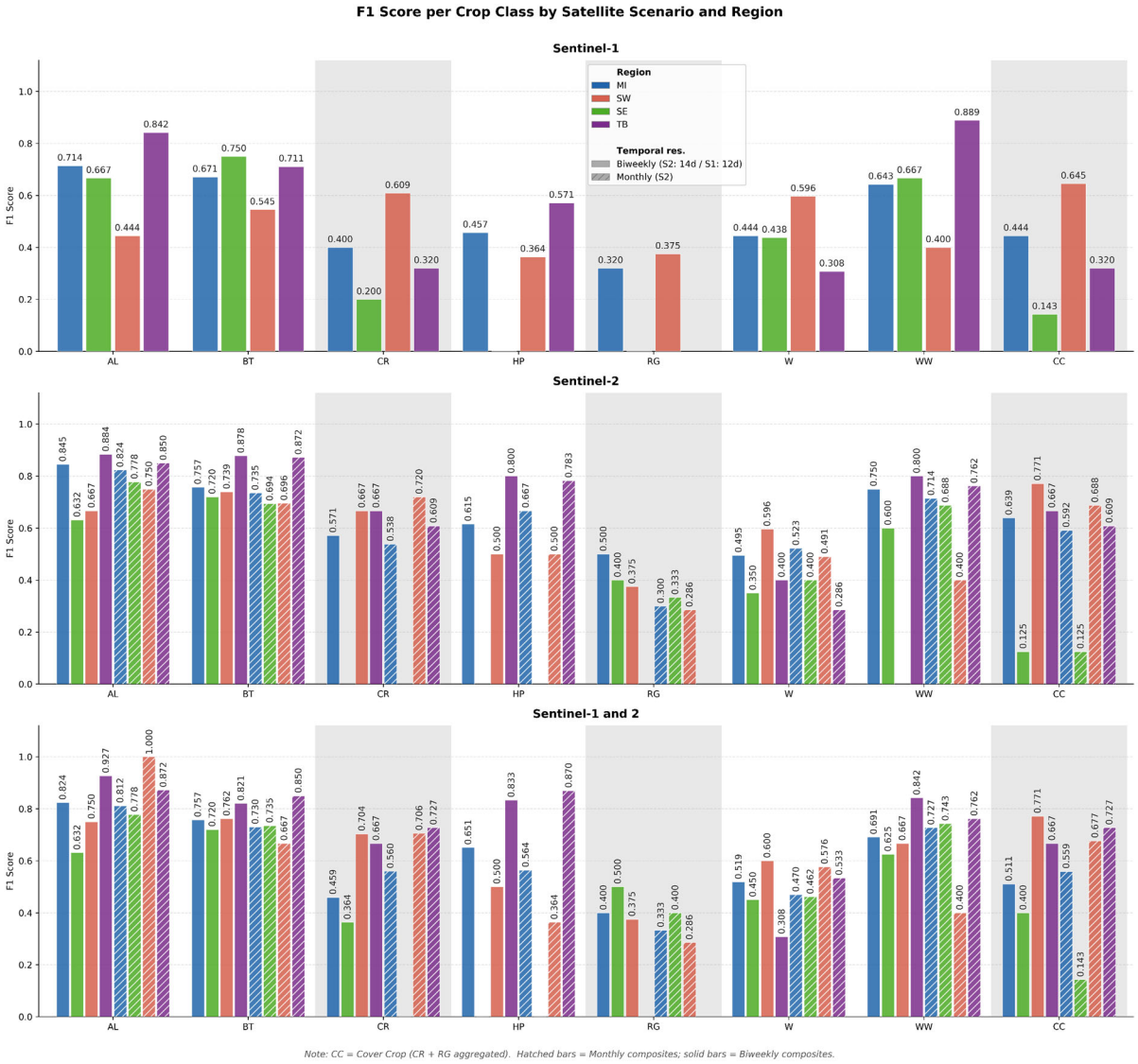


Figure 3. F1 scores for each land cover type in each model and region. Gray areas represent the F1 scores for each region for the two cover crop species (CR, RG) and the combination of cover crop species together (CC) across all models. BT = bare/tilled, W = weeds, CR = cereal rye, AL = alfalfa, WW = winter wheat, HP = hay forage/pasture, and RG = ryegrass. Sentinel-1 biweekly is always a 12-day quality mosaic; Sentinel-2 Biweekly is a 14-day quality mosaic.

While our accuracies for mapping cover crops may seem modest, they are higher than those from existing data products, specifically the USDA Cropland Data Layer (CDL), that map individual crop species across the continental United States. In the CDL, the UA and PA for cereal rye in 2019 in Michigan was 44.5% and 22.6%, respectively. Our models, on the other hand, achieved an accuracy of up to 52% for PA and 63% for UA when using 14-day mosaics of Sentinel-2 at the state level (Figures 4 and S8). Figure 5 shows examples of the polygon classification for the best models for each region and the comparison with CDL classes, highlighting regions where CR and RG are present in our classification but not in the CDL maps. Most of the areas classified as CR and RG in our model are classified as corn or soybean in the CDL (Figure S10).

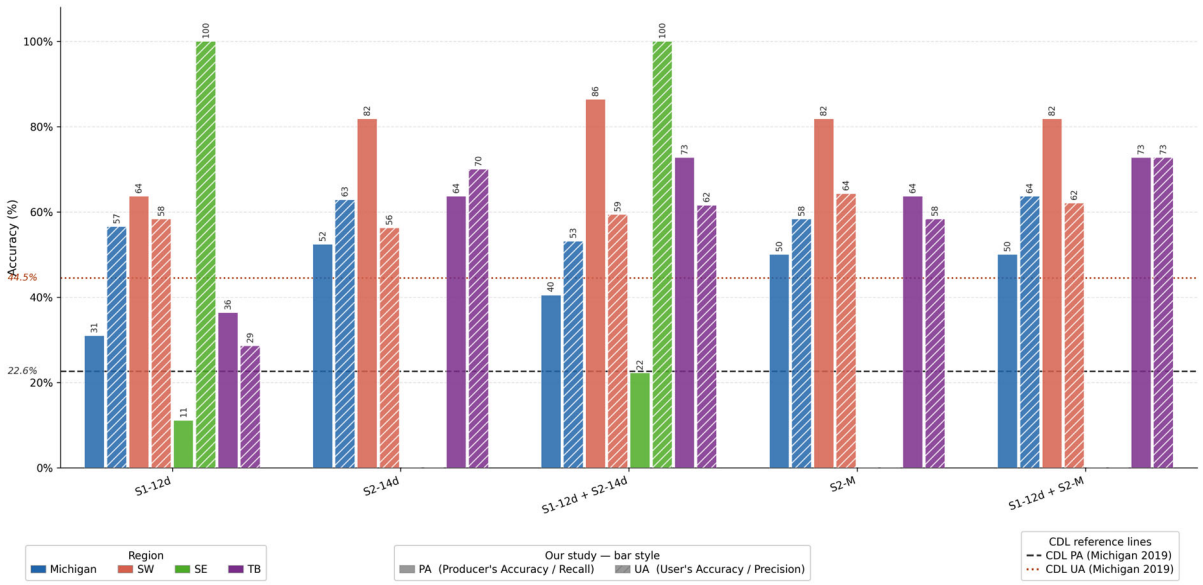


Figure 4. Comparison of user's and producer's accuracy from CDL and our models for cereal rye (CR).

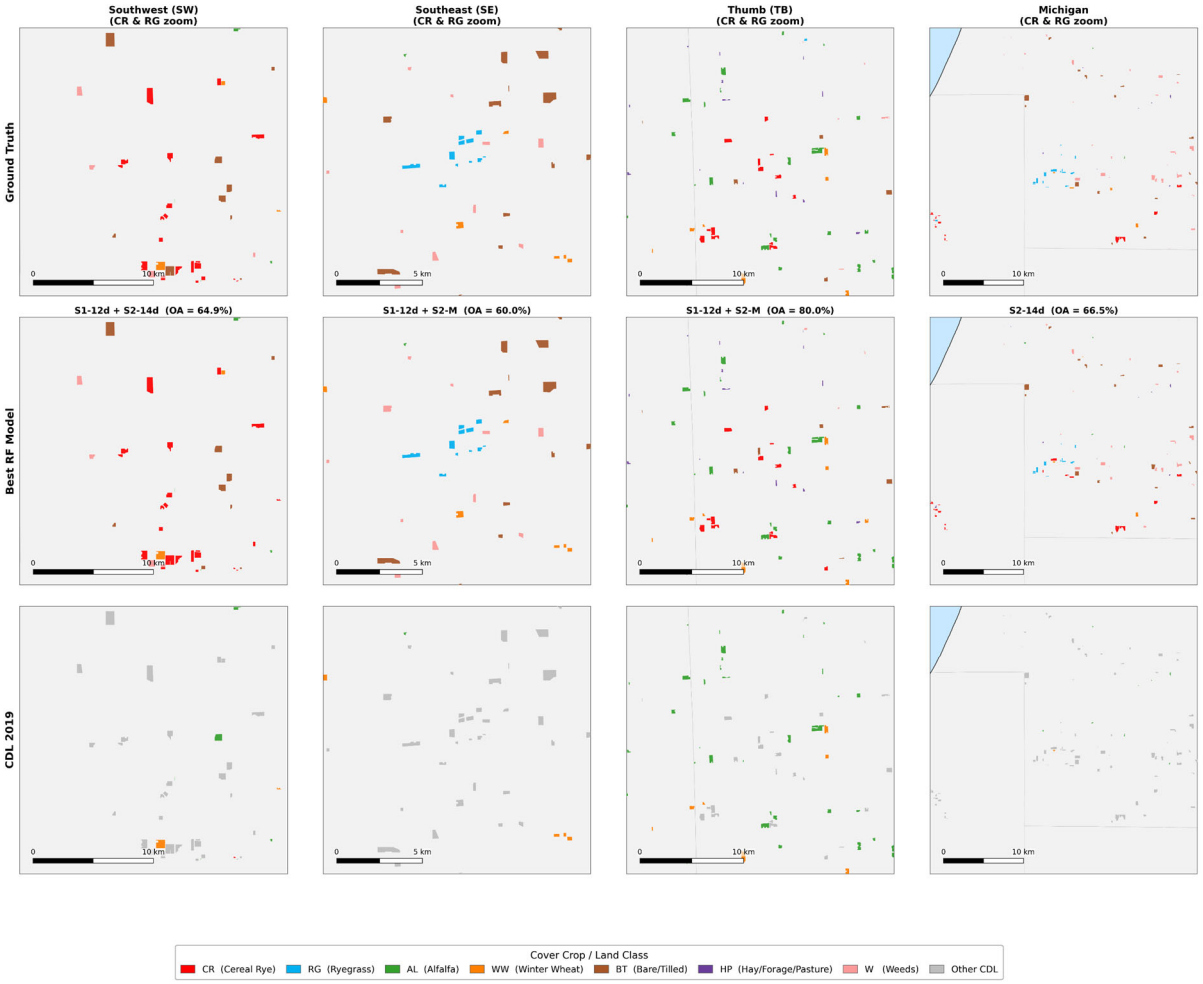


Figure 5. Comparison of predicted cereal rye (CR) and ryegrass (RG) in our models versus the CDL. All the classes from the CDL that did not match our classes are highlighted in gray.

3.2. Most Important Predictors to Map Winter Cover Types

To answer question 3, we examined which of the covariates (band, polarization and indices) were the most important in explaining model variance in each of our random forest models. Table S1 lists the top 5 most important variables across all models and Figure 6 represents the frequency of periods as well as the bands, polarizations, and indices among the five most important variables for each model. Variables from earlier in the growing season, particularly from the months of April and May, were the most common important predictors (Figure 6B,C), especially for the top two most important variables (Table S1). This is especially true for the models that include biweekly Sentinel-2 mosaics. Considering which bands and indices were the most important, we found that RVIm from early in the growing season was the most important variable in Sentinel-1 only models; however, its importance dropped in Sentinel-1 and Sentinel-2 combined models, with no Sentinel-1 bands or indices appearing as a top 5 most important factor in these combined models. However, Sentinel-1 variables still improved accuracies when combined with Sentinel-2 data (Table 4 and Figure 3), and Sentinel-1 RVIm is present as one of the most important variables when considering the top 20 features (Figure S5). In models that contain Sentinel-2 data, vegetation indices appear to be the most common important factors (Table S1 and Figure 6), particularly CIre which relies on Sentinel-2's two red edge bands (Table 1).

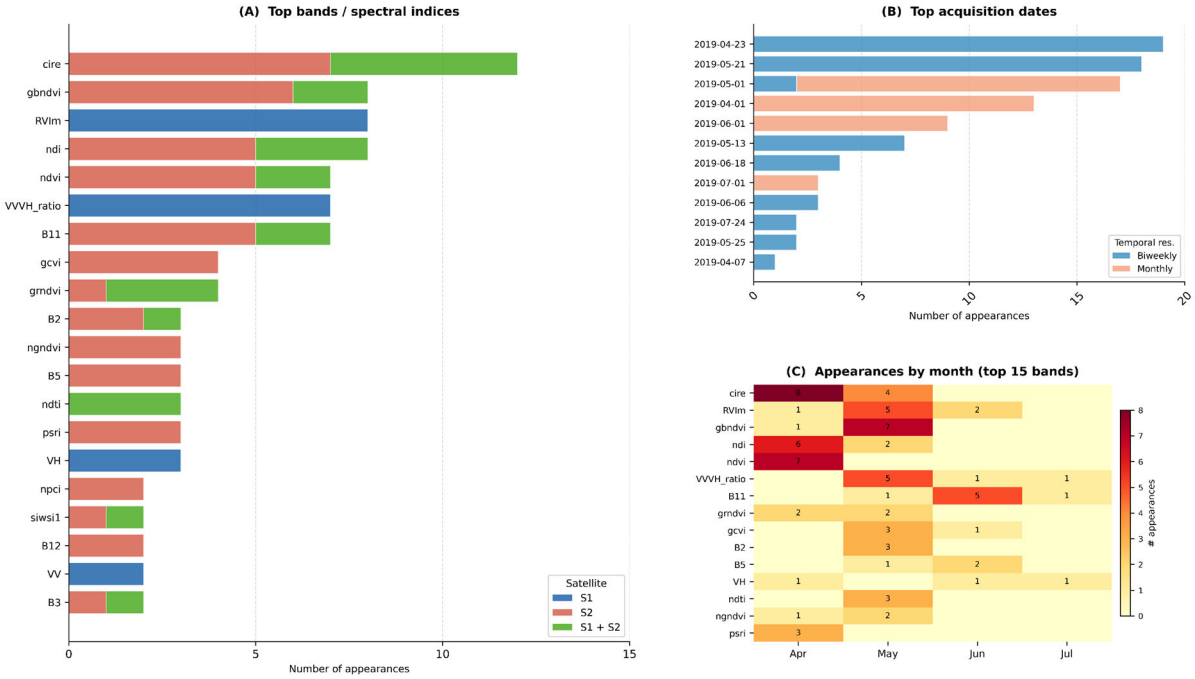


Figure 6. Feature importance summary for the 5 most important features for each model. Number of times that (**A**) each band/polarization/VI appeared; and (**B**) each period was repeated. The heatmap (**C**) represents the concentration of each band/feature for each month.

4. Discussion

We used Sentinel-1 and Sentinel-2 satellite data to map common types of winter plant cover, including cover crops, across agricultural landscapes in the lower Peninsula of Michigan. We examined (1) the extent to which including radar satellite data along with optical satellite data improved classification accuracy. We also (2) assessed whether a state-level, more generalizable model could be developed that had accuracies comparable to more localized, regional models. Finally, we examined (3) which bands, indices, polarizations, and time periods were the most important for classifying winter cover accurately. Overall,

we found that we were able to map winter cover with moderate accuracies (OA: 0.6 to 0.8) depending on region, with models that combine radar and optical data outperforming other models.

Considering question 1, models that combined Sentinel-1 and Sentinel-2 data generally had the highest accuracies. This is likely because there were gaps in the availability of Sentinel-2 imagery at the beginning of April in the southwest region, and at the start of May in all regions (Table 2). This is a key time period to identify overwintering cover crops that emerge in early spring or newly planted cover crops that are typically seeded in late April to mid-May. Sentinel-1 indices, such as RVIm that measure vegetation biomass and the VVVH_ratio, which measures backscatter intensity, were particularly important variables in May (Figure 6). These results suggest that radar data can provide key metrics of vegetation growth during periods of high cloud cover in the spring, improving model accuracy compared to using only optical data alone [67,68].

We found that overall accuracies varied across regions with the highest accuracies achieved for the thumb region and the lowest accuracies achieved for the southeast region (Table 4). There are several potential reasons for these differences in accuracy across regions. The thumb site may have had higher classification accuracies because the site did not contain any ryegrass (Figure 2), which was a difficult land cover to classify. The thumb also has greater crop rotation diversity and a larger number of organic farms, which allows for earlier planting of cereal rye and the potential for higher biomass production. The Southeast site is in Michigan's portion of the Western Lake Erie Basin, with agricultural landscapes in more intensive row crop production. In this region, cereal rye and ryegrass are planted in narrow windows within simplified corn–soybean rotations. Farmers may plant cereal rye late in the fall, or in some cases fly on the seed into a standing crop, both of which may lead to uneven establishment and poor cover crop growth. This site also had relatively fewer training polygons for most land cover classes, other than winter wheat, compared to the other two sites (Figure 2). Finally, the southwest site may have had higher overall accuracies because classification of difficult land cover classes, such as cereal rye and weeds, had moderate to high classification accuracies in this site. This region has a greater presence of vegetable and dairy farms, as well as seed corn production, which can offer longer periods for cover crop growth. We were able to collect increased training data for these two difficult land cover classes in the southwest region (Figure 2), likely due to higher prevalence across the landscape.

The classification accuracies varied greatly by land cover class, with the highest accuracies achieved for winter wheat (WW), alfalfa (AL), and bare/tilled (BT) fields, which is not surprising as these crops also achieve high accuracies in the CDL. The accuracies for the other land cover classes, including weeds (W), hay/pasture (HP), and cover crops (CC), were more mixed, with moderate to high accuracies in some regions and extremely poor accuracies in other regions. These general patterns likely occurred because the land covers that had mixed performance are heterogeneous considering planting times, harvest or termination times, and/or overall biomass production. This is especially the case for the cover crop species, which can have highly variable performance due to interactions between environmental conditions and management practices [69]. When considering F1 scores for cover crops, we found that accuracies varied based on cover crop type and region, and that a combined cover crop (CC) class (F1: 0.77) and cereal rye (CR) (F1: 0.73) achieved higher accuracy compared to ryegrass (RG) (F1: 0.5). Cereal rye is more commonly planted as a cover crop in Michigan and the Great Lakes region due to its cold tolerance and ability to establish in late fall after corn or soybean harvest [70], which was also evident in the larger sample size for cereal rye compared to ryegrass across our study regions.

Considering question 2, we found that our state-level model performed relatively well compared to the localized, regional models. While the state model (state: 0.66) underperforms the best regional model (TB: 0.80), its accuracy is better than or comparable to the localized models for the other two regions (SE: 0.60, SW: 0.65), with the state model slightly outperforming the best SW regional model (0.67 vs. 0.65). These results suggest that a more generalizable model that is trained across a diversity of soil types, management characteristics, and cover crop establishment methods can also do relatively well when mapping localized regions. It is likely that the reason the accuracy for the thumb region was higher was because there was no ryegrass in this region, which was the most difficult land cover class to predict. While we could not test our generalizable state model in regions outside of the three regions where it was trained due to a lack of ground data, we believe its ability in achieving a similar performance to locally trained models suggest that it is able to map winter cover well across a range of diverse soil, planting, and management conditions.

Considering which bands, polarizations, indices, and time periods were the most important for classification, we found that vegetation indices developed using the red edge bands were particularly important. CIre is found to be the most common variable across all models when considering only the top five most important variables (Table 4 and Figure 6A,C). This is not surprising given that previous studies have shown that the red edge bands are particularly useful in classifying different vegetation types [35,71]. Considering time periods, our results suggest that images earlier in the growing season (late April to early June) were more helpful for classifying winter cover (Figure 6B,C). This is because biomass growth (e.g,. NDVI) across the different land covers in our study differed the most during this time period (Figure S4). Finally, we found that from Sentinel-1, RVIm and the VVVH_ratio were the most helpful, particularly from early parts in the growing season. While these variables were never found in the top five variables in combined optical and radar models, RVIm was found in the top 20 most important features in combined models, suggesting that the improvement in model accuracy from adding radar data likely came most from this variable (Figure S5). This is likely because RVIm helped provide information about vegetation growth early in the growing season when optical datasets were unavailable due to cloud cover (e.g., during early April and May).

While our results suggest that it is possible to map winter cover with moderate accuracies using Sentinel-1 and Sentinel-2, there are several caveats and limitations that should be discussed. First, we only collected data for one year and in three regions, and it is unclear how generalizable our model is outside of these regions and in other years. Future work would benefit in testing the generalizability of our model and findings across space and time. Second, our collection of land cover ground truth points was not even as some land cover classes were less common across the landscape. Future work would benefit from understanding how much accuracies could be improved with a larger training dataset, particularly for the poorest performing classes, as training data limitations can cause substantial errors in maps created using machine learning algorithms [72,73]. Finally, while we find moderate accuracies across most of our models (approximately 0.65 for overall accuracy, and 0.77 for cover crops specifically), whether this accuracy is high enough to be useful will depend on the intended use case. For example, such accuracies may be sufficient for scientific inference, where errors will present themselves as noise, making the detection of statistically significant relationships conservative [74]. However, they may not be sufficient for monitoring and providing compensation to individual farmers who plant cover crops as part of a policy or subsidy scheme as many farmers would be incorrectly included or excluded from such programs, a concern echoed by recent critiques highlighting the shortcomings and misclassifications inherent when using remote sensing

for strict regulatory compliance [75]. Our data product, however, performs significantly better in mapping cover crops than existing available datasets such as the CDL (Figure 4).

5. Conclusions

This study examined the potential of multi-temporal Sentinel-1 and Sentinel-2 satellite imagery to map winter land cover types, including cover crop species, across three agriculturally distinct regions in the lower Peninsula of Michigan. We demonstrated that models that used both Sentinel-1 and Sentinel-2 data can map winter cover types with moderate accuracies that exceed those of existing data products that map cover crop types, such as the CDL. Our results also highlight that red edge vegetation indices and images acquired from late April to early June are the most informative for discriminating against winter cover types, providing practical guidance for the design of future mapping efforts. Future work should examine whether obtaining more training data for poorly performing classes, including cover crops, could improve accuracies by better capturing the heterogeneity in plant growth across the landscape.

Supplementary Materials: The following supporting information can be downloaded at: https://www.mdpi.com/article/10.3390/rs18121933/s1, Figure S1: Sentinel-2 biweekly cloud cover distribution for each region and for the entire state (aggregate). The x-axis represents the start day of the biweekly interval; Figure S2: Sentinel-2 monthly cloud cover distribution for each region and for the entire state (aggregate).The x-axis represents the start day of the monthly interval; Figure S3: Sentinel-1 biweekly cloud cover distribution for each region and for the entire state (aggregate).The x-axis represents the start day of the biweekly interval; Figure S4: Temporal boxplot distribution of the NDVI values for the biweekly mosaics for all polygons across Michigan; Figure S5: Feature importance summary for the 20 most important features for each model. Number of times that (A) each band/polarization/VI appeared; and (B) each period was repeated. The heatmap (C) represents the concentration of each band/feature for each month; Figure S6: Confusion matrices for state (Michigan) level and for each region (SW, SE, TB), considering the Sentinel-2 monthly (S2-M) and Sentinel-1 biweekly (S1-12d) data; Figure S7: Confusion matrices for state (Michigan) level and for each region (SW, SE, TB), considering the Sentinel-2 biweekly (S2-14d) and Sentinel-1 biweekly (S1-12d) data; Figure S8: User's and producer's accuracies for the state (Michigan) level and for each region (SW, SE, TB), considering the Sentinel-2 biweekly (S2-14d) and Sentinel-1 biweekly (S1-12d) data; Figure S9: User's and producer's accuracies for the state (Michigan) level and for each region (SW, SE, TB), considering the Sentinel-2 monthly (S2-M) and Sentinel-1 biweekly (S1-12d) data; Figure S10: CDL 2019 map for a representative area for each region and for Michigan. These areas are the same as those from Figure 5 in the main text; Table S1: F1 scores for each land cover type in each model and region. Bolded values represent the highest F1 scores for each region for the two cover crop species (CR, RG) and the combination of cover crop species together (CC) across all models; Table S2: The five most important variables for each model. Variables are listed as the date (yyyy-mm-dd), whether it is from a biweekly or monthly mosaic (b or m), and the band or index name.

Author Contributions: Conceptualization, J.B. and M.J.; methodology, Y.S., V.H.R.P., J.B., H.W., P.R. and M.J.; formal analysis, Y.S., V.H.R.P. and H.W.; investigation, Y.S. and V.H.R.P.; supervision, P.R. and M.J.; funding acquisition, J.B. and M.J.; writing—original draft preparation, Y.S. and V.H.R.P.; writing—review and editing, J.B., H.W., P.R. and M.J. All authors have read and agreed to the published version of the manuscript.

Funding: This work was supported by a USDA NIFA Grant (#2019-67019-29460) to J.B. and M.J.

Data Availability Statement: The satellite data utilized in this research are freely available from the sources described in the text. Field data for this study may be available from the corresponding author upon reasonable request.

Acknowledgments: The authors would like to acknowledge help from Xuewei Wang, Maanya Umashaanker, Divya Solomon, and Laurie Gronewold in identifying field location points and creating drive maps. We also would like to acknowledge Beth VanDusan, Etienne Sutton, Matthew Sutton, and Eliot Jackson for their work in collecting field data points.

Conflicts of Interest: The authors declare no conflict of interest.

References

1. Kessler, J.J.; Moolhuijzen, M. Low External Input Sustainable Agriculture: Expectations and Realities. *Neth. J. Agric. Sci.* **1994**, *42*, 181–194. [CrossRef]
2. Verma, A.K. Unsustainable Agriculture, Environmental Ethics and Ecological Balance. *HortFlora Res. Spectr.* **2018**, *7*, 239–241.
3. Blesh, J.; Drinkwater, L.E. The Impact of Nitrogen Source and Crop Rotation on Nitrogen Mass Balances in the Mississippi River Basin. *Ecol. Appl.* **2013**, *23*, 1017–1035. [CrossRef]
4. David, M.B.; Drinkwater, L.E.; McIsaac, G.F. Sources of Nitrate Yields in the Mississippi River Basin. *J. Environ. Qual.* **2010**, *39*, 1657–1667. [CrossRef] [PubMed]
5. Kerr, J.M.; DePinto, J.V.; McGrath, D.; Sowa, S.P.; Swinton, S.M. Sustainable Management of Great Lakes Watersheds Dominated by Agricultural Land Use. *J. Gt. Lakes Res.* **2016**, *42*, 1252–1259. [CrossRef]
6. Rabalais, N.N.; Turner, R.E. Gulf of Mexico Hypoxia: Past, Present, and Future. *Limnol. Oceanogr. Bull.* **2019**, *28*, 117–124. [CrossRef]
7. Lu, Y.-C.; Watkins, K.B.; Teasdale, J.R.; AIbdul-baki, A.A. Cover Crops in Sustainable Food Production. *Food Rev. Int.* **2000**, *16*, 121–157. [CrossRef]
8. Costa, A.; Bommarco, R.; Smith, M.E.; Bowles, T.; Gaudin, A.C.M.; Watson, C.A.; Alarcón, R.; Berti, A.; Blecharczyk, A.; Calderon, F.J.; et al. Crop Rotational Diversity Can Mitigate Climate-Induced Grain Yield Losses. *Glob. Change Biol.* **2024**, *30*, e17298. [CrossRef]
9. Bowles, T.M.; Mooshammer, M.; Socolar, Y.; Calderón, F.; Cavigelli, M.A.; Culman, S.W.; Deen, W.; Drury, C.F.; Garcia y Garcia, A.; Gaudin, A.C.M.; et al. Long-Term Evidence Shows That Crop-Rotation Diversification Increases Agricultural Resilience to Adverse Growing Conditions in North America. *One Earth* **2020**, *2*, 284–293. [CrossRef]
10. King, A.E.; Blesh, J. Crop Rotations for Increased Soil Carbon: Perenniality as a Guiding Principle. *Ecol. Appl.* **2018**, *28*, 249–261. [CrossRef]
11. Liebman, M.; Helmers, M.J.; Schulte, L.A.; Chase, C.A. Using Biodiversity to Link Agricultural Productivity with Environmental Quality: Results from Three Field Experiments in Iowa. *Renew. Agric. Food Syst.* **2013**, *28*, 115–128. [CrossRef]
12. Teasdale, J.R. Contribution of Cover Crops to Weed Management in Sustainable Agricultural Systems. *J. Prod. Agric.* **1996**, *9*, 475–479. [CrossRef]
13. Zhou, Q.; Guan, K.; Wang, S.; Jiang, C.; Huang, Y.; Peng, B.; Chen, Z.; Wang, S.; Hipple, J.; Schaefer, D.; et al. Recent Rapid Increase of Cover Crop Adoption Across the U.S. Midwest Detected by Fusing Multi-Source Satellite Data. *Geophys. Res. Lett.* **2022**, *49*, e2022GL100249. [CrossRef]
14. Surdoval, A.; Jain, M.; Blair, E.; Wang, H.; Blesh, J. Financial Incentive Programs and Farm Diversification with Cover Crops: Assessing Opportunities and Challenges. *Environ. Res. Lett.* **2024**, *19*, 044063. [CrossRef]
15. Cover Crop Trends, Programs, and Practices in the United States | Economic Research Service. Available online: https://www.ers.usda.gov/publications/pub-details?pubid=100550 (accessed on 11 February 2026).
16. Chami, B.; Niles, M.T.; Parry, S.; Mirsky, S.B.; Ackroyd, V.J.; Ryan, M.R. Incentive Programs Promote Cover Crop Adoption in the Northeastern United States. *Agric. Environ. Lett.* **2023**, *8*, e20114. [CrossRef]
17. Hively, W.D.; Duiker, S.; McCarty, G.; Prabhakara, K. Remote Sensing to Monitor Cover Crop Adoption in Southeastern Pennsylvania. *J. Soil Water Conserv.* **2015**, *70*, 340–352. [CrossRef]
18. Cruz-Ramírez, M.; Hervás-Martínez, C.; Jurado-Expósito, M.; López-Granados, F. A Multi-Objective Neural Network Based Method for Cover Crop Identification from Remote Sensed Data. *Expert Syst. Appl.* **2012**, *39*, 10038–10048. [CrossRef]
19. Sonobe, R.; Yamaya, Y.; Tani, H.; Wang, X.; Kobayashi, N.; Mochizuki, K. Mapping Crop Cover Using Multi-Temporal Landsat 8 OLI Imagery. *Int. J. Remote Sens.* **2017**, *38*, 4348–4361. [CrossRef]
20. Seifert, C.A.; Azzari, G.; Lobell, D.B. Satellite Detection of Cover Crops and Their Effects on Crop Yield in the Midwestern United States. *Environ. Res. Lett.* **2018**, *13*, 064033. [CrossRef]
21. Wang, X.; Blesh, J.; Rao, P.; Paliwal, A.; Umashaanker, M.; Jain, M. Mapping Cover Crop Species in Southeastern Michigan Using Sentinel-2 Satellite Data and Google Earth Engine. *Front. Artif. Intell.* **2023**, *6*, 1035502. [CrossRef]
22. Ahmed, Z.; Nalley, L.; Brye, K.; Steven Green, V.; Popp, M.; Shew, A.M.; Connor, L. Winter-Time Cover Crop Identification: A Remote Sensing-Based Methodological Framework for New and Rapid Data Generation. *Int. J. Appl. Earth Obs. Geoinf.* **2023**, *125*, 103564. [CrossRef]

23. Najem, S.; Baghdadi, N.; Bazzi, H.; Lalande, N.; Bouchet, L. Detection and Mapping of Cover Crops Using Sentinel-1 SAR Remote Sensing Data. *IEEE J. Sel. Top. Appl. Earth Obs. Remote Sens.* **2024**, *17*, 1446–1461. [CrossRef]
24. Gao, F.; Jennewein, J.; Hively, W.D.; Soroka, A.; Thieme, A.; Bradley, D.; Keppler, J.; Mirsky, S.; Akumaga, U. Near Real-Time Detection of Winter Cover Crop Termination Using Harmonized Landsat and Sentinel-2 (HLS) to Support Ecosystem Assessment. *Sci. Remote Sens.* **2023**, *7*, 100073. [CrossRef]
25. Jennewein, J.S.; Lamb, B.T.; Hively, W.D.; Thieme, A.; Thapa, R.; Goldsmith, A.; Mirsky, S.B. Integration of Satellite-Based Optical and Synthetic Aperture Radar Imagery to Estimate Winter Cover Crop Performance in Cereal Grasses. *Remote Sens.* **2022**, *14*, 2077. [CrossRef]
26. Barnes, M.L.; Yoder, L.; Khodaee, M. Detecting Winter Cover Crops and Crop Residues in the Midwest US Using Machine Learning Classification of Thermal and Optical Imagery. *Remote Sens.* **2021**, *13*, 1998. [CrossRef]
27. Zhou, Q.; Guan, K.; Wang, S.; Wu, X.; Stroebel, S.; Hipple, J. Multi-Sensor Assessment of Phenology-Based Field-Level Cover Cropping Detection Using Satellite Vegetation Time Series from Harmonized Landsat-8 and Sentinel-2, MODIS, and PlanetScope. *Int. J. Appl. Earth Obs. Geoinf.* **2026**, *146*, 105004. [CrossRef]
28. Fan, X.; Vrieling, A.; Muller, B.; Nelson, A. Winter Cover Crops in Dutch Maize Fields: Variability in Quality and Its Drivers Assessed from Multi-Temporal Sentinel-2 Imagery. *Int. J. Appl. Earth Obs. Geoinf.* **2020**, *91*, 102139. [CrossRef]
29. Gao, F.; Anderson, M.C.; Hively, W.D. Detecting Cover Crop End-Of-Season Using VENμS and Sentinel-2 Satellite Imagery. *Remote Sens.* **2020**, *12*, 3524. [CrossRef]
30. Prabhakara, K.; Hively, W.D.; McCarty, G.W. Evaluating the Relationship between Biomass, Percent Groundcover and Remote Sensing Indices across Six Winter Cover Crop Fields in Maryland, United States. *Int. J. Appl. Earth Obs. Geoinf.* **2015**, *39*, 88–102. [CrossRef]
31. Breunig, F.M.; Galvão, L.S.; Dalagnol, R.; Dauve, C.E.; Parraga, A.; Santi, A.L.; Della Flora, D.P.; Chen, S. Delineation of Management Zones in Agricultural Fields Using Cover–Crop Biomass Estimates from PlanetScope Data. *Int. J. Appl. Earth Obs. Geoinf.* **2020**, *85*, 102004. [CrossRef]
32. Thieme, A.; Yadav, S.; Oddo, P.C.; Fitz, J.M.; McCartney, S.; King, L.; Keppler, J.; McCarty, G.W.; Hively, W.D. Using NASA Earth Observations and Google Earth Engine to Map Winter Cover Crop Conservation Performance in the Chesapeake Bay Watershed. *Remote Sens. Environ.* **2020**, *248*, 111943. [CrossRef]
33. Demir, Z.; Tursun, N.; Isik, D. Effects of Different Cover Crops on Soil Quality Parameters and Yield in an Apricot Orchard. *Int. J. Agric. Biol.* **2019**, *21*, 399–408.
34. Frasier, I.; Quiroga, A.; Noellemeyer, E. Effect of Different Cover Crops on C and N Cycling in Sorghum NT Systems. *Sci. Total Environ.* **2016**, *562*, 628–639. [CrossRef]
35. Clevers, J.G.P.W.; Gitelson, A.A. Remote Estimation of Crop and Grass Chlorophyll and Nitrogen Content Using Red-Edge Bands on Sentinel-2 and -3. *Int. J. Appl. Earth Obs. Geoinf.* **2013**, *23*, 344–351. [CrossRef]
36. Kc, K.; Zhao, K.; Romanko, M.; Khanal, S. Assessment of the Spatial and Temporal Patterns of Cover Crops Using Remote Sensing. *Remote Sens.* **2021**, *13*, 2689. [CrossRef]
37. Song, X.-P.; Huang, W.; Hansen, M.C.; Potapov, P. An Evaluation of Landsat, Sentinel-2, Sentinel-1 and MODIS Data for Crop Type Mapping. *Sci. Remote Sens.* **2021**, *3*, 100018. [CrossRef]
38. Tricht, K.V.; Gobin, A.; Gilliams, S.; Piccard, I. Synergistic Use of Radar Sentinel-1 and Optical Sentinel-2 Imagery for Crop Mapping: A Case Study for Belgium. *Remote Sens.* **2018**, *10*, 1642. [CrossRef]
39. Denize, J.; Hubert-Moy, L.; Betbeder, J.; Corgne, S.; Baudry, J.; Pottier, E. Evaluation of Using Sentinel-1 and -2 Time-Series to Identify Winter Land Use in Agricultural Landscapes. *Remote Sens.* **2018**, *11*, 37. [CrossRef]
40. Selvaraj, S.; Bargiel, D.; Htitiou, A.; Gerighausen, H. Analyzing Temporal Characteristics of Winter Catch Crops Using Sentinel-1 Time Series. *Remote Sens.* **2024**, *16*, 3737. [CrossRef]
41. Jensch, K.; Ghazaryan, G.; Ernst, S.; Hostert, P.; Nendel, C. Integrating Landsat, Sentinel-2 and Sentinel-1 Time Series for Mapping Intermediate Crops. *Eur. J. Remote Sens.* **2025**, *58*, 2507738. [CrossRef]
42. Shao, Y. Cover Crop Mapping in Lower Peninsula of Michigan State Using Harmonized Landsat 8 and Sentinel-2 (HLS) Data. Master's Thesis, University of Michigan, Ann Arbor, MI, USA, 2021.
43. Rouse, W.; Haas, R.H.; Schell, J.A.; Deering, D.W. Monitoring Vegetation Systems in the Great Plains with ERTS. In *Proceedings of the Third Earth Resources Technology Satellite-1 Symposium*; Volume 1: Technical Presentations, section A; NASA Goddard Space Flight Center: Greenbelt, MD, USA, 1974; pp. 309–317.
44. United States Department of Agriculture (USDA); National Agricultural Statistics Service (NASS). USDA, National Agricultural Statistics Service, 2018 Cultivated Layer. Available online: https://www.nass.usda.gov/Research_and_Science/Cropland/metadata/2018_cultivated_layer_metadata.htm (accessed on 25 August 2022).
45. Gorelick, N.; Hancher, M.; Dixon, M.; Ilyushchenko, S.; Thau, D.; Moore, R. Google Earth Engine: Planetary-Scale Geospatial Analysis for Everyone. *Remote Sens. Environ.* **2017**, *202*, 18–27. [CrossRef]

46. Sentinel-2 Cloud Masking with S2cloudless | Google Earth Engine | Google Developers. Available online: https://developers.google.com/earth-engine/tutorials/community/sentinel-2-s2cloudless (accessed on 25 August 2022).
47. Skakun, S.; Wevers, J.; Brockmann, C.; Doxani, G.; Aleksandrov, M.; Batič, M.; Frantz, D.; Gascon, F.; Gómez-Chova, L.; Hagolle, O.; et al. Cloud Mask Intercomparison eXercise (CMIX): An Evaluation of Cloud Masking Algorithms for Landsat 8 and Sentinel-2. *Remote Sens. Environ.* **2022**, *274*, 112990. [CrossRef]
48. Mullissa, A.; Vollrath, A.; Odongo-Braun, C.; Slagter, B.; Balling, J.; Gou, Y.; Gorelick, N.; Reiche, J. Sentinel-1 SAR Backscatter Analysis Ready Data Preparation in Google Earth Engine. *Remote Sens.* **2021**, *13*, 1954. [CrossRef]
49. Tucker, C.J. Red and Photographic Infrared Linear Combinations for Monitoring Vegetation. *Remote Sens. Environ.* **1979**, *8*, 127–150. [CrossRef]
50. Wang, F.; Huang, J.; Chen, L. Development of a Vegetation Index for Estimation of Leaf Area Index Based on Simulation Modeling. *J. Plant Nutr.* **2010**, *33*, 328–338. [CrossRef]
51. Wang, F.; Huang, J.; Tang, Y.; Wang, X. New Vegetation Index and Its Application in Estimating Leaf Area Index of Rice. *Rice Sci.* **2007**, *14*, 195–203. [CrossRef]
52. Pérez, A.J.; López, F.; Benlloch, J.V.; Christensen, S. Colour and Shape Analysis Techniques for Weed Detection in Cereal Fields. *Comput. Electron. Agric.* **2000**, *25*, 197–212. [CrossRef]
53. Merzlyak, M.N.; Gitelson, A.A.; Chivkunova, O.B.; Rakitin, V.Y. Non-Destructive Optical Detection of Pigment Changes during Leaf Senescence and Fruit Ripening. *Physiol. Plant.* **1999**, *106*, 135–141. [CrossRef]
54. Qi, J.; Marsett, R.; Heilman, P.; Bieden-bender, S.; Moran, S.; Goodrich, D.; Weltz, M. RANGES Improves Satellite-Based Information and Land Cover Assessments in Southwest United States. *EOS Trans. Am. Geophys. Union* **2002**, *83*, 601–606. [CrossRef]
55. Gitelson, A.A.; Gritz, Y.; Merzlyak, M.N. Relationships between Leaf Chlorophyll Content and Spectral Reflectance and Algorithms for Non-Destructive Chlorophyll Assessment in Higher Plant Leaves. *J. Plant Physiol.* **2003**, *160*, 271–282. [CrossRef] [PubMed]
56. Penuelas, J.; Pinol, J.; Ogaya, R.; Filella, I. Estimation of Plant Water Concentration by the Reflectance Water Index WI (R900/R970). *Int. J. Remote Sens.* **1997**, *18*, 2869–2875. [CrossRef]
57. Fensholt, R.; Sandholt, I. Derivation of a Shortwave Infrared Water Stress Index from MODIS Near- and Shortwave Infrared Data in a Semiarid Environment. *Remote Sens. Environ.* **2003**, *87*, 111–121. [CrossRef]
58. Van Deventer, A.P.; Ward, A.D.; Gowda, P.M.; Lyon, J.G. Using Thematic Mapper Data to Identify Contrasting Soil Plains and Tillage Practices. *Photogramm. Eng. Remote Sens.* **1997**, *63*, 87–93.
59. Mandal, D.; Kumar, V.; Ratha, D.; Dey, S.; Bhattacharya, A.; Lopez-Sanchez, J.M.; McNairn, H.; Rao, Y.S. Dual Polarimetric Radar Vegetation Index for Crop Growth Monitoring Using Sentinel-1 SAR Data. *Remote Sens. Environ.* **2020**, *247*, 111954. [CrossRef]
60. Breiman, L. Random Forests. *Mach. Learn.* **2001**, *45*, 5–32. [CrossRef]
61. Pedregosa, F.; Varoquaux, G.; Gramfort, A.; Michel, V.; Thirion, B.; Grisel, O.; Blondel, M.; Prettenhofer, P.; Weiss, R.; Dubourg, V.; et al. Scikit-Learn: Machine Learning in Python. *J. Mach. Learn. Res.* **2011**, *12*, 2825–2830.
62. Bargiel, D. A New Method for Crop Classification Combining Time Series of Radar Images and Crop Phenology Information. *Remote Sens. Environ.* **2017**, *198*, 369–383. [CrossRef]
63. Lantz, B. *Machine Learning with R: Learn How to Use R to Apply Powerful Machine Learning Methods and Gain an Insight into Real-World Applications*; Community experience distilled; Packt Pub.: Birmingham, UK, 2013.
64. Lebourgeois, V.; Dupuy, S.; Vintrou, É.; Ameline, M.; Butler, S.; Bégué, A. A Combined Random Forest and OBIA Classification Scheme for Mapping Smallholder Agriculture at Different Nomenclature Levels Using Multisource Data (Simulated Sentinel-2 Time Series, VHRS and DEM). *Remote Sens.* **2017**, *9*, 259. [CrossRef]
65. Olofsson, P.; Foody, G.M.; Stehman, S.V.; Woodcock, C.E. Making Better Use of Accuracy Data in Land Change Studies: Estimating Accuracy and Area and Quantifying Uncertainty Using Stratified Estimation. *Remote Sens. Environ.* **2013**, *129*, 122–131. [CrossRef]
66. Olofsson, P.; Foody, G.M.; Herold, M.; Stehman, S.V.; Woodcock, C.E.; Wulder, M.A. Good Practices for Estimating Area and Assessing Accuracy of Land Change. *Remote Sens. Environ.* **2014**, *148*, 42–57. [CrossRef]
67. Valero, S.; Arnaud, L.; Planells, M.; Ceschia, E. Synergy of Sentinel-1 and Sentinel-2 Imagery for Early Seasonal Agricultural Crop Mapping. *Remote Sens.* **2021**, *13*, 4891. [CrossRef]
68. Caballero, G.; Pezzola, A.; Winschel, C.; Angonova, P.S.; Casella, A.; Orden, L.; Salinero-Delgado, M.; Reyes-Muñoz, P.; Berger, K.; Delegido, J.; et al. Synergy of Sentinel-1 and Sentinel-2 Time Series for Cloud-Free Vegetation Water Content Mapping with Multi-Output Gaussian Processes. *Remote Sens.* **2023**, *15*, 1822. [CrossRef]
69. Sutton, E.; Blesh, J. Citizen Science Reveals Opportunities for Improving Sustainability Outcomes of Cover Crops. *J. Soil Water Conserv.* **2026**, *80*, 693–708. [CrossRef]
70. CTIC-SARE-ASTA. *National Cover Crop-Survey 2022–23*; Conservation Technology Information Center: West Lafayette, Indiana, 2023.

71. Schuster, C.; Förster, M.; Kleinschmit, B. Testing the Red Edge Channel for Improving Land-Use Classifications Based on High-Resolution Multi-Spectral Satellite Data. *Int. J. Remote Sens.* **2012**, *33*, 5583–5599. [CrossRef]
72. Elmes, A.; Alemohammad, H.; Avery, R.; Caylor, K.; Eastman, J.R.; Fishgold, L.; Friedl, M.A.; Jain, M.; Kohli, D.; Bayas, J.C.L.; et al. Accounting for Training Data Error in Machine Learning Applied to Earth Observations. *Remote Sens.* **2020**, *12*, 1034. [CrossRef]
73. Prudente, V.H.R.; Skakun, S.; Oldoni, L.V.; Xaud, H.A.M.; Xaud, M.R.; Adami, M.; Sanches, I.D. Multisensor Approach to Land Use and Land Cover Mapping in Brazilian Amazon. *ISPRS J. Photogramm. Remote Sens.* **2022**, *189*, 95–109. [CrossRef]
74. Jain, M. The Benefits and Pitfalls of Using Satellite Data for Causal Inference. *Rev. Environ. Econ. Policy* **2020**, *14*, 157–169. [CrossRef]
75. van der Velden, D.; Klerkx, L.; Dessein, J.; Debruyne, L. Governance by Satellite: Remote Sensing, Bureaucrats and Agency in the Common Agricultural Policy of the European Union. *J. Rural Stud.* **2025**, *114*, 103558. [CrossRef]

Disclaimer/Publisher's Note: The statements, opinions and data contained in all publications are solely those of the individual author(s) and contributor(s) and not of MDPI and/or the editor(s). MDPI and/or the editor(s) disclaim responsibility for any injury to people or property resulting from any ideas, methods, instructions or products referred to in the content.